Three-Dimensional Imaging and Quantification of Both Solitary Cells and Metastases in Whole Mouse Liver by Magnetic Resonance Imaging

Jason L. Townson,[1,4] Soha S. Ramadan,[2] Carmen Simedrea,[1] Brian K. Rutt,[2,4] Ian C. MacDonald,[4] Paula J. Foster,[2,4] and Ann F. Chambers[1,3,4]

[1]London Regional Cancer Program; [2]Robarts Research Institute, [3]Department of Oncology, and [4]Department of Medical Biophysics, University of Western Ontario, London, Ontario, Canada

Abstract

The metastatic cell population, ranging from solitary cells to actively growing metastases, is heterogeneous and unlikely to respond uniformly to treatment. However, quantification of the entire experimental metastatic cell population in whole organs is complicated by requirements of an imaging modality with the large field of view and high spatial resolution necessary to detect both single cells and metastases in the same organ. Thus, it is difficult to assess differential responses of these distinct metastatic populations to therapy. Here, we develop a magnetic resonance imaging (MRI) technique capable of quantifying the full population of metastatic cells in a secondary organ. B16F1 mouse melanoma cells were labeled with micron-sized iron oxide particles (MPIO) and injected into mouse liver via the mesenteric vein. Livers were removed immediately or at day 9 or 11, following doxorubicin or vehicle control treatment, and imaged using a 3T clinical magnetic resonance scanner and custom-built gradient coil. Both metastases (>200 μm) and MPIO-labeled single cells were detected and quantified from MR images as areas of hyperintensity or hypointensity (signal voids), respectively. We found that 1 mg/kg doxorubicin treatment inhibited metastasis growth (n = 11 per group; P = 0.02, t test) but did not decrease the solitary metastatic cell population in the same livers (P > 0.05). Thus, the technique presented here is capable of quickly quantifying the majority of the metastatic cell population, including both growing metastases and solitary cells, in whole liver by MRI and can identify differential responses of growing metastases and solitary cells to therapy. [Cancer Res 2009;69(21):8326–31]

Introduction

Successful treatment of metastatic disease remains a significant clinical challenge, with treatment failure often attributed to tumor inaccessibility, advanced stage of the disease upon detection, poor drug delivery, or drug resistance (1–3). However, experimental metastasis models have revealed that the population of metastatic cells within a secondary organ is heterogeneous and unlikely to respond uniformly to treatment (4–8). This situation was shown by Naumov and colleagues who showed that doxorubicin was able to inhibit growth of large vascularized metastases but had no effect on the number or viability of solitary dormant cells present in the same organs or their ability to subsequently form metastases (5). Ultimate treatment failure in patients therefore may also be the result of failure to target the entire population of metastatic cells, particularly solitary dormant cells. However, experimental studies of solitary dormant metastatic cells and development of treatments to target them are complicated by the difficulties associated with detecting and quantifying single cells *in vivo*.

Several imaging modalities have been used to study metastasis. The advantages and limitations of these modalities, including positron emission tomography, single-photon emission computed tomography, computed tomography, magnetic resonance (MR), ultrasound, and bioluminescent and fluorescent optical imaging, are well documented (9–14). To date, the majority of studies focusing specifically on solitary metastatic cells have relied on fluorescent optical imaging due primarily to the high-resolution capabilities of this modality. In fact, the dormant metastatic cell population has been defined by optical characteristics including retention of exogenous fluorescent markers that are diluted and no longer visible following a few cycles of replication (5, 7, 8, 15). However, although fluorescent optical imaging has been used most frequently and provides the most detailed resolution for the study of single cells *in vivo*, the restricted field of view and depth of penetration often limit attempts to quantify solitary metastatic cells as well as growing metastases distributed throughout an entire organ or animal. In addition, this method can be destructive to the tissue and samples only a small subset of the organ.

Advances in cellular magnetic resonance imaging (MRI) have provided a powerful imaging modality by which single cells can be detected and quantified noninvasively on a scale ranging from small tissue samples to whole animals (9, 16–19). Heyn and colleagues showed that solitary cells, including cancer cells, could be detected in mouse brain by MRI when labeled with iron oxide particles (MPIO; refs. 16, 18). These cells appear in MR images as signal voids (areas of image hypointensity; that is, black) due to the susceptibility effect and increased local relaxivity caused by the iron oxide particles with which the cells are labeled (17, 18). Using the same three-dimensional fast imaging employing steady-state acquisition pulse sequenced used here, it has also been shown that, as MPIO-labeled cells begin to proliferate, the areas of hypointensity are lost due to dilution of label with cell division (18). Metastases that subsequently form in the same location are visible in images as areas of hyperintensity (that is, white) without additional contrast agent (18). Labeling MDA-MB-231BR breast cancer cells with MPIO was shown previously to have no effect on the growth of the cells *in vitro* or their subsequent ability to form brain metastases in mice (18). Comparison of MR images and histologic sections confirmed that signal voids in MR images corresponded

Note: Supplementary data for this article are available at Cancer Research Online (http://cancerres.aacrjournals.org/).

Requests for reprints: Ann F. Chambers, London Regional Cancer Program, 790 Commissioners Road East, Office A4-903B, London, Ontario, Canada N6A 4L6. Phone: 519-685-8652; Fax: 519-685-8646; E-mail: ann.chambers@Lhsc.on.ca.

doi:10.1158/0008-5472.CAN-09-1496

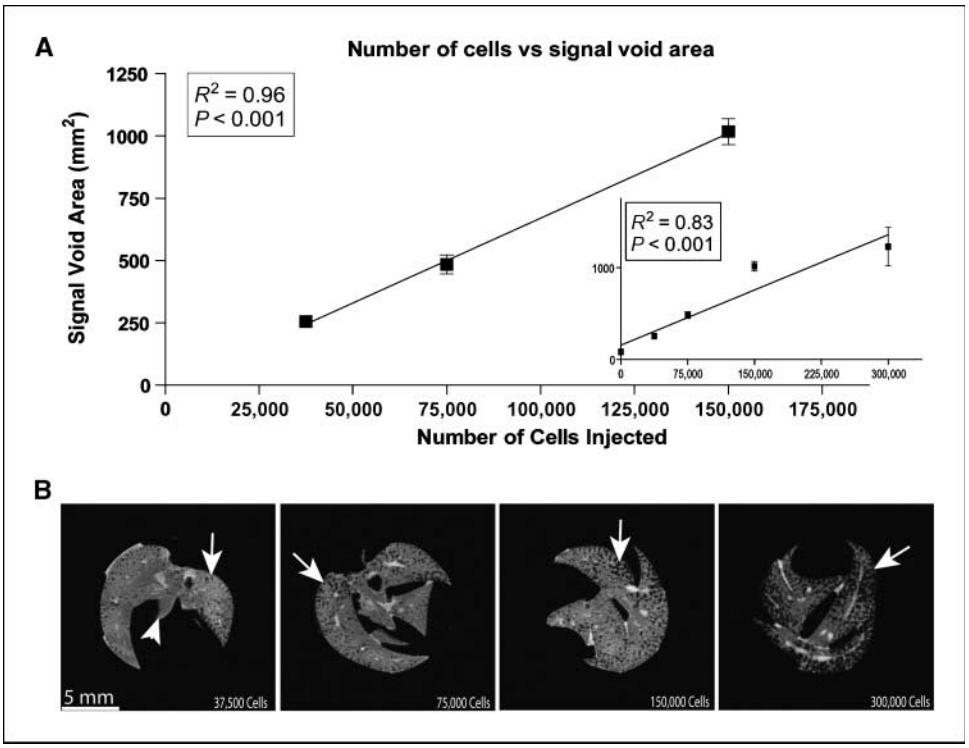

Figure 1. Signal void area strongly correlates with the number of MPIO-labeled B16F1 cells in the liver. A strong correlation (R^2 = 0.96; P < 0.001) exists between the number of cells injected and the total signal void area detected in whole mouse livers (*A*). This correlation covers the range from 3.75×10^4 to 1.5×10^5 cells. For the entire range between 0 and 3×10^5 cells, the R^2 correlation is 0.83 (P < 0.001; *inset*). *B*, MPIO-labeled B16F1 cells are apparent in MR images as multiple signal voids (dark spots; e.g., *arrows*) in a background of normal liver tissue that appears gray (e.g., *arrowhead*). An increase in the number and size of signal voids is apparent in the representative MR images of an increasing number of cells (3.75×10^4, 7.5×10^4, 1.5×10^5, and 3.0×10^5).

with sections in the brain where fluorescent MPIO-labeled cancer cells were present (18). In addition, Shapiro and colleagues showed that individual MPIO-labeled hepatocytes could be detected in liver following migration from the spleen (17). However, the utility of cellular MRI techniques for quantifying the effect of a cancer treatment on the entire metastatic cell population in whole organs has not yet been shown.

Here, we describe a MRI method by which the majority of the metastatic population of B16F1 melanoma cells in mouse liver, including both solitary cells and growing metastases, can be rapidly (<6 min scan per liver) quantified in intact livers while preserving the tissue for further analysis. This novel method of quantification was then used to determine the effect of doxorubicin on both solitary cells and growing metastases. It was found that doxorubicin significantly decreased total metastatic tumor volume but failed to reduce the number of solitary dormant metastatic cells in the same livers.

Materials and Methods

Cell culture and MPIO labeling. Cell culture and MPIO labeling procedures were similar to those described previously (8, 18). Briefly, B16F1 murine melanoma cells were maintained in α-MEM containing 10% fetal bovine serum at 37°C and 5% CO_2. For MPIO labeling, cells were grown in a T75 tissue culture flask using medium with fetal bovine serum until 80% to 90% confluent. MPIO beads (312.5 μL supplied stock suspension, 0.9 μm diameter, 63% magnetite, labeled with Dragon Green; Bangs Laboratory) were then added to 10 mL medium with fetal bovine serum per flask and incubated for 24 h. The cells were washed thoroughly with serum-free α-MEM to remove unincorporated MPIO beads. Cells were then centrifuged and resuspended in serum-free α-MEM at the appropriate concentration for injection. Nearly all cells were efficiently labeled with MPIO, and labeling did not inhibit cell growth *in vitro* or the ability of cells to form metastases *in vivo* (data not shown) as reported previously (18).

Experimental metastasis assay and doxorubicin treatment. Female, 6- to 10-week-old C57BL/6 mice (Harlan) were cared for in accordance with the Canadian Council on Animal Care under a protocol approved by the University of Western Ontario Council on Animal Care. For experimental metastasis assays, mice were anesthetized with an i.p. injection of xylazine/ketamine (2.6 mg ketamine and 0.13 mg xylazine per 20 g body mass). Anesthetized mice received mesenteric vein injections of 100 μL B16F1 cells suspended in α-MEM to target cells directly to liver as described (8). It has been shown previously that the majority of cells injected via this route are trapped in the liver by size restriction in liver sinusoids, with ~90% of injected cells retained in the liver 90 min after injection (8). To quantify how signal void volume varies with the number of cells in the liver (proportional to the number of cells injected), mice (3-4 per group; total n = 14) were injected with 3.75×10^4, 7.5×10^4, 1.5×10^5, or 3.0×10^5 cells per mouse (in 100 μL) and sacrificed 10 to 15 min following cell injection. For tumor burden and treatment experiments, 3×10^5 B16F1 cells (in 100 μL) were injected. Livers to be scanned and correlated with MR images were removed at day 11. Treatment with doxorubicin (Pharmacia) at 1 mg/kg, or vehicle control (0.9% sodium chloride), commenced 24 h following cell injection and continued three times weekly for a total of four treatments. Mice (n = 11 control and n = 11 treated) were sacrificed 9 days following cell injection and livers were removed and fixed in formalin for at least 48 h.

MRI and image analysis. Mice were sacrificed and livers removed immediately (10-15 min) or at 9 days (doxorubicin experiment) or 11 days (histology correlation) following cell injection. Formalin-fixed livers were scanned using a 3T clinical MRI. All MRI examinations were done on a 3T GE CV/i whole-body clinical magnetic resonance scanner as described previously (18). In brief, this included a custom-built gradient coil (inner diameter 12 cm, maximum gradient strength 600 mT/m, and peak slew rate 2,000 T/m/s) and solenoidal radiofrequency coil (inner diameter 1.5 cm). Images were obtained using the three-dimensional fast imaging employing steady-state acquisition pulse sequence (20). The scanned resolution was 100 × 100 × 200 μm^3 and the total acquisition time was <6 min per whole liver. No additional contrast agent (other than MPIO in cells) was used in these studies. This single-cell MRI approach thus differs from most other contrast agent approaches in the liver (primarily gadolinium-based agents), which are intended to improve detection of metastases, whereas our approach is intended to permit detection of solitary cells before commencement of proliferation.

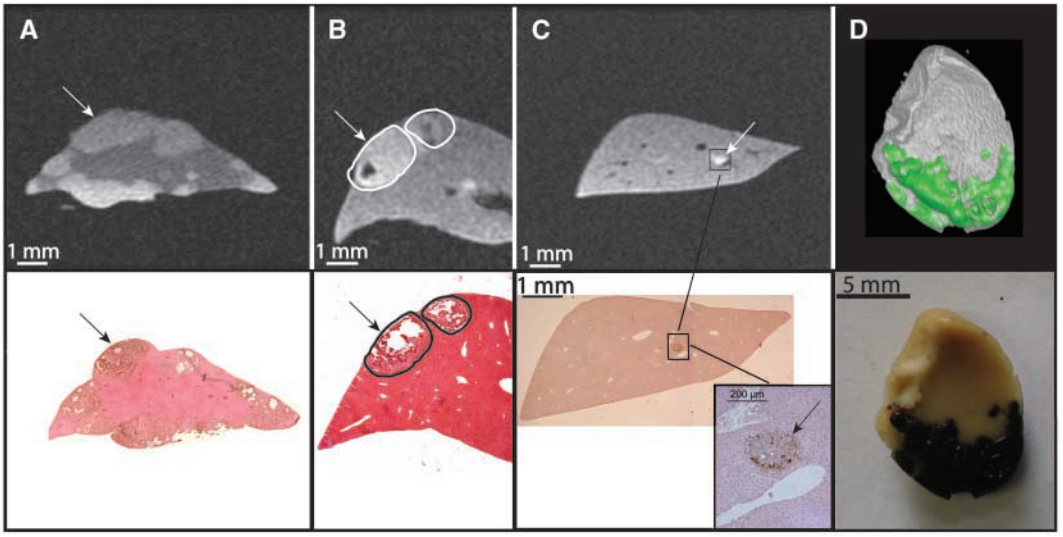

Figure 2. MR image hyperintensity corresponds with metastatic tissue in histologic sections. Hyperintense regions (*white arrows*) in MR images (*A* and *B, top*) correlate with regions of B16F1 metastatic tumors (*black arrows*) in H&E-stained histologic sections (*A* and *B, bottom*). B16F1 metastases as small as 200 μm were apparent in MR images (*C, top*) and corresponded with small metastases visible in histologic sections (*C, bottom*). Two-dimensional MR images (*A-C, top*), which sample the entire liver, can be used to render representative three-dimensional images in which tumor is apparent (pseudocolored green; *D, top*). Three-dimensional rendering of liver closely resembles the picture of the scanned liver lobe (*D, bottom*).

Tumor and liver volume analysis and three-dimensional reconstruction of images were completed using VGStudio Max (Volume Graphics) or OsiriX imaging software (open source). This process is semiautomated as hyperintense areas of images were automatically thresholded and subsequent manual correction of misclassified regions (such as vasculature) was done. Signal void area was measured using ImageJ image analysis software (NIH). For each group of mice, a pixel value threshold was established manually and subsequent analysis for all scans within each experiment was automatically calculated using the fixed-pixel intensity threshold. At least 125 images per organ were used to calculate signal void area.

Histology and statistics. Digital images of whole formalin-fixed livers were acquired using a 7.1 MP digital camera (Canon) mounted to a tripod. These were used for comparison of visible surface tumors with surface-rendered MRI images of hyperintense regions. For histologic correlation, livers were paraffin-embedded, sectioned (4 μm), and stained with H&E.

Statistical analysis of tumor volume and signal void area following doxorubicin treatment was done using a *t* test comparing volume and area (respectively) from at least 125 MR images per liver. Data are presented as mean ± SE. A standard curve and R^2 value were generated by linear regression and used to quantify the correlation between signal void area and the number of solitary cells present in the liver. All statistical analyses were done using GraphPad Prism software.

Results

MRI signal void area strongly correlates with the number of MPIO-labeled cells. To determine if MRI signal void area could be used to quantify the number of cells present in the liver, we assessed the correlation between signal void area and the number of B16F1 cells labeled with MPIO in that organ (Fig. 1). Varying numbers (3×10^5, 1.5×10^5, 7.5×10^4, or 3.75×10^4) of B16F1 cells labeled with MPIO were delivered to mouse liver via mesenteric vein injection. Livers were removed immediately following injections, fixed in formalin, and scanned by 3T MRI as described in Materials and Methods. As seen in Fig. 1*B*, it is readily apparent that both the number and area of signal voids (*arrows*) increases with the number of cells injected into the liver. The coefficient of determination (R^2) value between signal void area and cell number over the entire range of cells injected from 0 to 300,000 was 0.83 ($P < 0.001$; Fig. 1*A, inset*). However, within the range between

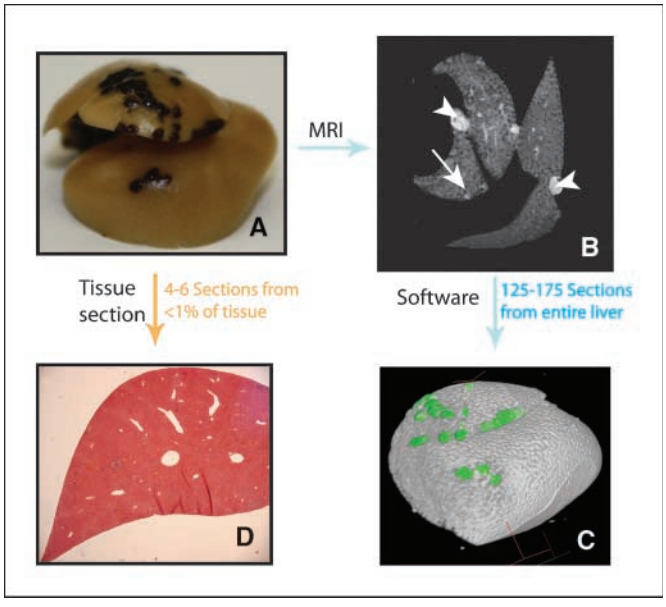

Figure 3. Diagram showing how MR images of entire liver can be used to calculate multiple tumor, solitary cells, and liver parameters. Whole livers (*A*) can be scanned by magnetic resonance to generate two-dimensional images (100 × 100 × 200 μm resolution) from which signal void area is calculated (*B*). Two-dimensional MRI sections (125-175 spanning entire liver) can be used to render three-dimensional images (*C*) from which volume measurements can be made (see also Supplementary Video 1). A limited number of random or representative histologic sections (*D*) are generally used to determine tumor and solitary cell data. MR image data can be used to calculate multiple variables that are restricted in analysis of histologic sections.

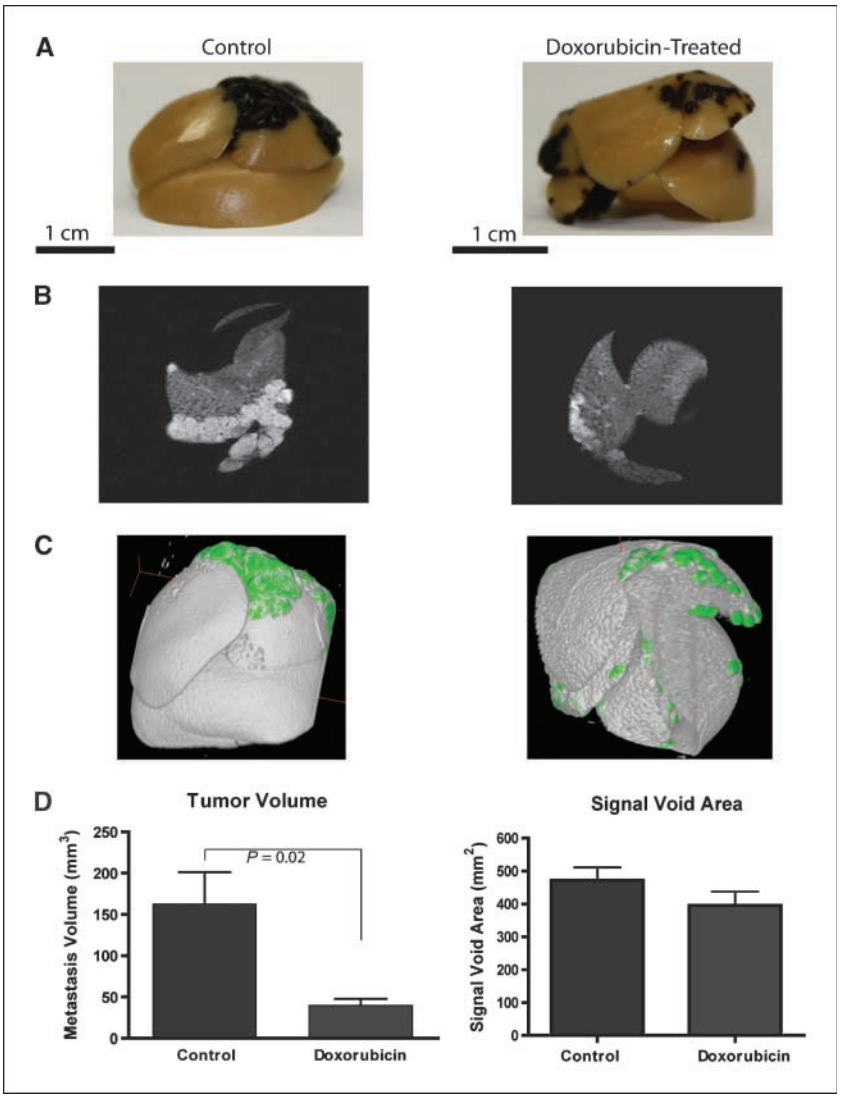

Figure 4. Doxorubicin inhibited growth of metastases but did not decrease the number of dormant cells as measured by signal void area. Whole livers, showing black melanotic tumors visible at the liver surface (*A*), were scanned by MRI producing multiple two-dimensional images (representative images, *B*) sampling the entire liver. Two-dimensional images were combined to render three-dimensional volumetric images of the originally scanned livers (*C*). A decrease in surface tumor is visible as a decrease in black or green false coloring in *A* and *C*, respectively. Decreased area of hyperintensity (tumor tissue) was apparent in two-dimensional MR images (*B*) of doxorubicin-treated mice. Quantification of signal void area from two-dimensional images and metastatic tumor volume from three-dimensional images showed that doxorubicin treatment resulted in a significant decrease in tumor volume ($n = 11$ per treatment group; $P = 0.02$, *t* test; *D*). However, doxorubicin treatment did not decrease the number of dormant cells in the same livers ($P = 0.2$, *t* test) as quantified by MR signal void area at endpoint (*D*).

3.75×10^4 and 1.5×10^5 cells, R^2 increased to 0.96 ($P < 0.001$; Fig. 1*A*). A decrease of 3.75×10^4 cells (between 3.75×10^4 and 7.5×10^4 cells), representing only 12.5% of number of cells initially injected, was found to be significantly different ($P = 0.0019$, *t* test) within a population of only 8 mice. The high degree of correlation between the number of MPIO-labeled cells and signal void area (cell number explaining up to 96% of the variance in signal void area) indicates that quantification of this MR image parameter is a useful measure of the number of cells and ultimately quantification of the effect of treatment on this population of cells.

Quantification of B16F1 liver metastases (hyperintensity) in MR images. To assess the utility of the 6 min whole-liver 3T MRI scan for quantification of liver metastasis volume, unlabeled B16F1 cells were injected into liver via mesenteric vein. Livers were removed at day 11 following injection and imaged by MR as described above. As seen in Fig. 2*A* and *B*, tumor tissue in histologic images (*bottom*), from which tumor burden, area, or size have traditionally been quantified, is readily apparent as areas of hyperintensity in corresponding MR images (*top*). Tumor tissue hyperintensity from metastases as small as 200 μm in diameter, by histology, were also visible in MR images (Fig. 2*C*). The appearance of tumor tissue as hyperintense regions in the liver is consistent with previous publications using T2-weighted images (21–23). Tumor hyperintensity can be used to calculate multiple tumor parameters, including volume, and can also be used to segment the tissue into multiple regions of interest that can be used to render three-dimensional images. Three-dimensional images rendered using semiautomated segmentation based on tumor tissue hyperintensity closely resemble whole scanned liver lobes as can be seen by the surface tumor pattern (Fig. 2*D*).

Metastases and solitary dormant cells are apparent in the same MR image. To determine the feasibility of quantifying both solitary cells and growing metastases from the same MR images, livers injected with MPIO-labeled B16F1 cells were removed and imaged at day 9. Whole intact livers (Fig. 3*A*) were scanned by MRI as described above. This resulted in two-dimensional images (Fig. 3*B*) in which both signal voids (*arrow*) from MPIO-labeled B16F1 cells and hyperintense areas (*arrowheads*) from metastases could be seen in the same image. The two-dimensional images were then used to render a three-dimensional image (Fig. 3*C*; Supplementary Video S1) of the whole liver with surface tumor patterns similar to those of the intact whole liver (Fig. 3*A*). As the entire liver volume is scanned, MR images can be used to quantify size, number, and total tumor and normal tissue volume

information from the whole liver (Fig. 3). All metastases in the organ can be assessed in contrast to the limited number of representative sections that are routinely assessed with histology (Fig. 3*D*). In addition, this rapid MRI scanning procedure is nondestructive, so tissue is preserved for further analysis following the scans.

Doxorubicin decreased metastatic tumor volume but not signal void area. To assess the ability of the MRI technique described here to quantify the effect of doxorubicin on both growing metastases and the solitary dormant metastatic cell population in whole mouse liver, 3×10^5 B16F1 cells labeled with MPIO were injected into the liver via the mesenteric vein. Mice were treated with 1 mg/kg doxorubicin, or vehicle control, three times weekly (four total treatments). Livers were removed 9 days after cell injection, fixed, and scanned by MRI as above. Doxorubicin treatment resulted in an obvious decrease in surface tumor area in whole-liver images (Fig. 4*A*), three-dimensional MR image rendering, and two-dimensional MR image tumor area (hyperintensity; Fig. 4*B* and *C*). Analysis of MR images showed that doxorubicin treatment resulted in a significant decrease in metastatic tumor volume ($n = 11$ per group; $P = 0.02$, t test; Fig. 4*D, left*). However, doxorubicin treatment did not decrease the number of solitary cells in the same livers ($P = 0.2$, t test) as quantified by MR signal void area at endpoint (Fig. 4*D, right*). The mean signal void area from all livers at endpoint (434 ± 29 mm^2) corresponds with $6.5 \times 10^4 \pm 5.8 \times 10^3$ cells (Fig. 1*A*). MR images were also analyzed to determine the total number of metastases, liver volume, total liver and tumor volume, and average metastasis volume for all livers (Supplementary Fig. S1). The results of this experiment thus show the utility of this rapid MRI technique in simultaneously assessing the effect of treatment on solitary tumor cells and metastases and show that doxorubicin has a differential effect on metastases and solitary tumor cells, inhibiting metastatic growth but not affecting the number of solitary tumor cells in the same livers.

Discussion

Here, we present a novel MRI method that allows rapid quantification of the majority of the metastatic cell population, including both solitary cells and growing metastases, in a whole organ from a single scan while preserving the tissue for further analysis. Using this technique, we showed that doxorubicin treatment significantly inhibited B16F1 metastatic tumor growth but had no effect on the number of solitary dormant metastatic cells present in the same livers. Several studies have shown that a larger proportion of metastatic cells may remain as solitary dormant cells compared with those that grow to form large vascularized metastases (4, 7, 8, 24–26). However, although the single-cell population may be clinically important and at least in part responsible for delayed recurrences, this population of cells remains poorly understood (5, 27). The MRI quantification method outlined here allows for rapid assessment of drug efficacy on a much greater proportion of the metastatic cell population, inclusive of both metastases and solitary dormant cells, compared with other currently available methods of quantification.

Multiple MRI-based techniques are currently used to detect and quantify iron oxide–labeled cells (19). These include detection of iron-labeled hepatocytes, macrophages, dendritic, cancer, and stem cells using T1-, T2-, and T2*-weighted imaging techniques and quantification using multiple MRI parameters including T2, R2, and R2* (20, 28–35). It has been established qualitatively that the number of MPIO-labeled human breast cancer cells delivered to the brain is associated with the number of MRI signal voids (18). In addition, it has been shown that the spatial arrangement of signal voids found in MR images of the brain and liver corresponded with cellular fluorescence from MPIO-labeled cells in these tissues (17, 18). Signal voids present in the brain and liver 28 or 30 days following injection, respectively, were previously verified to be due to the originally injected cells, which had been dual-labeled with both fluorescent dyes and superparagmagnetic iron (17, 18). In contrast, experiments in which killed MPIO-labeled cells or free MPIO were injected into the spleen or liver resulted in signal void patterns and intensity of signal loss that differed substantially from those observed in mice injected with viable MPIO-labeled cells (17). In the day 9 MR images of livers from the doxorubicin treatment experiment in the present study, some smaller less hypointense areas of signal void were also observed. It is likely that at least some of these signal voids in which hypointensity peaks are not as pronounced may be due to MPIO that is no longer concentrated in the originally injected solitary cells. However, as the signal void area is quantified here based on a set threshold value, the difference in the intensity of signal loss can be used to exclude these areas of weak signal loss from the endpoint quantification. Further, based on the magnitude of signal void loss shown here at endpoint, less than one-third of the originally injected cell population remained. This is consistent with past experiments with the B16F1 cell line in which cell fate was assessed by optical techniques (8). Taken together, our current results, as well those published previously (17, 18), thus suggest that the signal voids quantified here represent iron-retaining cancer cells.

Due to signal void "blooming" (MRI signal void appearing much larger than the actual MPIO-labeled cells) and the proximity of cells to one another, a single MRI signal void is not always due to a single cell (16, 36). This appears to be observable in Fig. 1 where the size and number of signal voids increase with cell number. As may be expected (see Fig. 1, *inset*), at higher cell numbers, some signal voids will overlap, resulting in a nonlinear relationship between signal void area and numbers of cells injected. However, here we show that there is a strong correlation (R^2 values = 0.83-0.96) between signal void area in MR images and the number of metastatic cells present in the liver, indicating that signal void area is proportional to numbers of single cells present. This correlation is especially high ($R^2 = 0.96$) in the range between 3.75×10^4 and 1.5×10^5 cells (12.5-50% of cells initially injected). This is important as results from experimental metastasis models in which solitary cell fate has been quantified have shown that this is the range within which the number of solitary dormant metastatic cells would most commonly be expected to fall (5, 7, 8). Consistent with this, we found that total signal void area from MPIO-labeled B16F1 cells at day 9 accounted for a much smaller ($\sim 6.5 \times 10^4$), however still significant, proportion of the 3×10^5 cells initially injected.

Our finding that doxorubicin treatment inhibited metastasis growth but did not decrease the number of solitary MPIO-labeled B16F1 cells (Fig. 4) is in agreement with results of a previous experiment in which mouse mammary carcinoma cells were quantified by fluorescent optical imaging (5). That study also showed that doxorubicin inhibited metastatic burden while not affecting the numbers of single cells present. Although the full significance of the dormant metastatic cell population remains to be understood,

it is likely that exclusion of this population of metastatic cells from analysis of treatment efficacy plays a role in treatment failure leading to recurrence (5, 15, 27, 37–40). A growing number of metastasis models have shown that solitary dormant metastatic cells retain their capacity to proliferate, forming late-growing metastases or primary tumors following isolation and reinjection (4, 7, 8, 16, 24–26). The quantification method we present here advances the study of treatment effect on metastatic cells, as it is currently the only method we are aware of that possesses the capability to detect, localize, and quantify the majority of the metastatic cell population in whole organs without destroying the tissue and while preserving a three-dimensional digital record. Currently, only a small proportion of the metastatic cell population is sampled to determine the effect of treatment in most studies. Taking into consideration the heterogeneous nature of the metastatic cell population, it may not be possible to develop treatments capable of fully eliminating metastatic disease until the effect of any compound on the entire population is understood. The method that we present here represents an opportunity to assess the effect of treatment on a significant population of metastatic cells that may be responsible for often significant failure rates in treatment of metastatic disease.

Disclosure of Potential Conflicts of Interest

No potential conflicts of interest were disclosed.

Acknowledgments

Received 4/23/09; revised 8/21/09; accepted 9/8/09; published OnlineFirst 10/20/09.

Grant support: Canadian Institutes of Health Research grant 42511 (A.F. Chambers and I.C. MacDonald) and doctoral research award (J.L. Townson). A.F. Chambers is Canada Research Chair in Oncology and receives salary support from the Canada Research Chairs Program.

The costs of publication of this article were defrayed in part by the payment of page charges. This article must therefore be hereby marked *advertisement* in accordance with 18 U.S.C. Section 1734 solely to indicate this fact.

References

1. Goldie JH, Coldman AJ. The genetic origin of drug resistance in neoplasms: implications for systemic therapy. Cancer Res 1984;44:3643–53.
2. Agarwal R, Kaye SB. Ovarian cancer: strategies for overcoming resistance to chemotherapy. Nat Rev Cancer 2003;3:502–16.
3. Van den Broeck A, Sergeant G, Ectors N, Van Steenbergen W, Aerts R, Topal B. Patterns of recurrence after curative resection of pancreatic ductal adenocarcinoma. Eur J Surg Oncol 2009;35:600–4.
4. Goodison S, Kawai K, Hihara J, et al. Prolonged dormancy and site-specific growth potential of cancer cells spontaneously disseminated from nonmetastatic breast tumors as revealed by labeling with green fluorescent protein. Clin Cancer Res 2003;9:3808–14.
5. Naumov GN, Townson JL, MacDonald IC, et al. Ineffectiveness of doxorubicin treatment on solitary dormant mammary carcinoma cells or late-developing metastases. Breast Cancer Res Treat 2003;82:199–206.
6. Chambers AF, Groom AC, MacDonald IC. Dissemination and growth of cancer cells in metastatic sites. Nat Rev Cancer 2002;2:563–72.
7. Cameron MD, Schmidt EE, Kerkvliet N, et al. Temporal progression of metastasis in lung: cell survival, dormancy, and location dependence of metastatic inefficiency. Cancer Res 2000;60:2541–6.
8. Luzzi KJ, MacDonald IC, Schmidt EE, et al. Multistep nature of metastatic inefficiency: dormancy of solitary cells after successful extravasation and limited survival of early micrometastases. Am J Pathol 1998;153:865–73.
9. Weissleder R, Pittet MJ. Imaging in the era of molecular oncology. Nature 2008;452:580–9.
10. Hoffman RM. *In vivo* real-time imaging of nuclear-cytoplasmic dynamics of dormancy, proliferation and death of cancer cells. APMIS 2008;116:716–29.
11. Graham KC, Ford NL, MacKenzie LT, et al. Noninvasive quantification of tumor volume in preclinical liver metastasis models using contrast-enhanced X-ray computed tomography. Invest Radiol 2008;43:92–9.
12. Sahai E. Illuminating the metastatic process. Nat Rev Cancer 2007;7:737–49.
13. Graham KC, Wirtzfeld LA, MacKenzie LT, et al. Three-dimensional high-frequency ultrasound imaging for longitudinal evaluation of liver metastases in preclinical models. Cancer Res 2005;65:5231–7.
14. Wirtzfeld LA, Graham KC, Groom AC, et al. Volume measurement variability in three-dimensional high-frequency ultrasound images of murine liver metastases. Phys Med Biol 2006;51:2367–81.
15. Naumov GN, MacDonald IC, Chambers AF, Groom AC. Solitary cancer cells as a possible source of tumour dormancy? Semin Cancer Biol 2001;11:271–6.
16. Heyn C, Ronald JA, Mackenzie LT, et al. *In vivo* magnetic resonance imaging of single cells in mouse brain with optical validation. Magn Reson Med 2006;55:23–9.
17. Shapiro EM, Sharer K, Skrtic S, Koretsky AP. *In vivo* detection of single cells by MRI. Magn Reson Med 2006;55:242–9.
18. Heyn C, Ronald JA, Ramadan SS, et al. *In vivo* MRI of cancer cell fate at the single-cell level in a mouse model of breast cancer metastasis to the brain. Magn Reson Med 2006;56:1001–10.
19. Liu W, Frank J. Detection and quantification of magnetically labeled cells by cellular MRI. Eur J Radiol 2008;70:258–64.
20. Foster-Gareau P, Heyn C, Alejski A, Rutt BK. Imaging single mammalian cells with a 1.5 T clinical MRI scanner. Magn Reson Med 2003;49:968–71.
21. Qin Y, Van Cauteren M, Osteaux M, Willems G. Quantitative study of the growth of experimental hepatic tumors in rats by using magnetic resonance imaging. Int J Cancer 1992;51:665–70.
22. Qin Y, Van Cauteren M, Osteaux M, Schally AV, Willems G. Inhibitory effect of somatostatin analogue RC-160 on the growth of hepatic metastases of colon cancer in rats: a study with magnetic resonance imaging. Cancer Res 1992;52:6025–30.
23. Namasivayam S, Martin DR, Saini S. Imaging of liver metastases: MRI. Cancer Imaging 2007;7:2–9.
24. Naumov GN, MacDonald IC, Weinmeister PM, et al. Persistence of solitary mammary carcinoma cells in a secondary site: a possible contributor to dormancy. Cancer Res 2002;62:2162–8.
25. Logan PT, Fernandes BF, Di Cesare S, Marshall JA, Maloney SC, Burnier MNJ. Single-cell tumor dormancy model of uveal melanoma. Clin Exp Metastasis 2008;25:509–16.
26. Suzuki M, Mose ES, Montel V, Tarin D. Dormant cancer cells retrieved from metastasis-free organs regain tumorigenic and metastatic potency. Am J Pathol 2006;169:673–81.
27. Goss P, Allan AL, Rodenhiser DI, Foster PJ, Chambers AF. New clinical and experimental approaches for studying tumor dormancy: does tumor dormancy offer a therapeutic target? APMIS 2008;116:552–68.
28. Rad AM, Arbab AS, Iskander ASM, Jiang Q, Soltanian-Zadeh H. Quantification of superparamagnetic iron oxide (SPIO)-labeled cells using MRI. J Magn Reson Imaging 2007;26:366–74.
29. de Vries IJM, Lesterhuis WJ, Barentsz JO, et al. Magnetic resonance tracking of dendritic cells in melanoma patients for monitoring of cellular therapy. Nat Biotechnol 2005;23:1407–13.
30. Bos C, Delmas Y, Desmoulière A, et al. *In vivo* MR imaging of intravascularly injected magnetically labeled mesenchymal stem cells in rat kidney and liver. Radiology 2004;233:781–9.
31. Hauger O, Frost EE, van Heeswijk R, et al. MR evaluation of the glomerular homing of magnetically labeled mesenchymal stem cells in a rat model of nephropathy. Radiology 2006;238:200–10.
32. Liu W, Dahnke H, Rahmer J, Jordan EK, Frank JA. Ultrashort T(2) (*) relaxometry for quantitation of highly concentrated superparamagnetic iron oxide (SPIO) nanoparticle labeled cells. Magn Reson Med 2009;61:761–6.
33. Arbab AS, Janic B, Knight RA, et al. Detection of migration of locally implanted AC133$^+$ stem cells by cellular magnetic resonance imaging with histological findings. FASEB J 2008;22:3234–46.
34. Dekaban GA, Snir J, Shrum B, et al. Semiquantitation of mouse dendritic cell migration *in vivo* using cellular MRI. J Immunother 2009;32:240–51.
35. Foster PJ, Dunn EA, Karl KE, et al. Cellular magnetic resonance imaging: *in vivo* imaging of melanoma cells in lymph nodes of mice. Neoplasia 2008;10:207–16.
36. Dodd SJ, Williams M, Suhan JP, Williams DS, Koretsky AP, Ho C. Detection of single mammalian cells by high-resolution magnetic resonance imaging. Biophys J 1999;76:103–9.
37. Demicheli R, Biganzoli E, Boracchi P, Greco M, Retsky MW. Recurrence dynamics does not depend on the recurrence site. Breast Cancer Res 2008;10:R83.
38. Schewe DM, Aguirre-Ghiso JA. ATF6α-Rheb-mTOR signaling promotes survival of dormant tumor cells *in vivo*. Proc Natl Acad Sci U S A 2008;105:10519–24.
39. Aguirre-Ghiso JA. Models, mechanisms and clinical evidence for cancer dormancy. Nat Rev Cancer 2007;7:834–46.
40. Townson JL, Chambers AF. Dormancy of solitary metastatic cells. Cell Cycle 2006;5:1744–50.